Metamorphosis of Sn 2014c: Delayed Interaction Between a Hydrogen Poor Core-Collapse Supernova and a Nearby Circumstellar Shell

Accepted to The Astrophysical Journal, October 26, 2015
Preprint typeset using LaTeX style emulateapj v. 5/2/11

METAMORPHOSIS OF SN 2014C: DELAYED INTERACTION BETWEEN A HYDROGEN POOR CORE-COLLAPSE SUPERNOVA AND A NEARBY CIRCUMSTELLAR SHELL

D. Milisavljevic[1], R. Margutti[1], A. Kamble[1], D. J. Patnaude[1], J. C. Raymond[1], J. J. Eldridge[2], W. Fong[3,4], M. Bietenholz[5,6], P. Challis[1], R. Chornock[7], M. R. Drout[1], C. Fransson[8], R. A. Fesen[9], J. E. Grindlay[1], R. P. Kirshner[1], R. Lunnan[1], J. Mackey[10], G. F. Miller[1], J. T. Parrent[1], N. E. Sanders[1], A. M. Soderberg[1], B. A. Zauderer[1]

Accepted to The Astrophysical Journal, October 26, 2015

ABSTRACT

We present optical observations of supernova SN 2014C, which underwent an unprecedented slow metamorphosis from H-poor type Ib to H-rich type IIn over the course of one year. The observed spectroscopic evolution is consistent with the supernova having exploded in a cavity before encountering a massive shell of the progenitor star's stripped hydrogen envelope. Possible origins for the circumstellar shell include a brief Wolf-Rayet fast wind phase that overtook a slower red supergiant wind, eruptive ejection, or confinement of circumstellar material by external influences of neighboring stars. An extended high velocity Hα absorption feature seen in near-maximum light spectra implies that the progenitor star was not completely stripped of hydrogen at the time of core collapse. Archival pre-explosion Subaru Telescope Suprime-Cam and Hubble Space Telescope Wide Field Planetary Camera 2 images of the region obtained in 2009 show a coincident source that is most likely a compact massive star cluster in NGC 7331 that hosted the progenitor system. By comparing the emission properties of the source with stellar population models that incorporate interacting binary stars we estimate the age of the host cluster to be $30-300$ Myr, and favor ages closer to 30 Myr in light of relatively strong Hα emission. SN 2014C is the best-observed member of a class of core-collapse supernovae that fill the gap between events that interact strongly with dense, nearby environments immediately after explosion and those that never show signs of interaction. Better understanding of the frequency and nature of this intermediate population can contribute valuable information about the poorly understood final stages of stellar evolution.

Subject headings: supernovae: general — supernova: individual (SN 2014C)

1. INTRODUCTION

Recent observations have convincingly demonstrated that massive stars can experience an eruptive mass loss episode $\sim$ 1 yr before core collapse. Such episodes have been confirmed in H-rich type IIn (Ofek et al. 2013; Smith et al. 2014; Ofek et al. 2014) and H-poor, He-rich type Ibn (Pastorello et al. 2007; Foley et al. 2007) supernovae. Although the brief timescales between eruption and supernova explosion have been anticipated in special cases of very massive stars (Woosley et al. 2007; Quataert & Shiode 2012), a growing number of systems are being discovered that fall outside most theoretical regimes and that challenge many long held notions of stellar evolution (Stritzinger et al. 2012; Pastorello et al. 2013; Mauerhan et al. 2013; Margutti et al. 2014; Smith & Arnett 2014; Moriya 2015).

The most favored candidate progenitors of type IIn and Ibn supernovae are luminous blue variable (LBV) stars (Kotak & Vink 2006; Pastorello et al. 2007; Gal-Yam & Leonard 2009), and stars leaving the LBV phase and entering a Wolf-Rayet (W-R) phase (Smith et al. 2012; Pastorello et al. 2015) that may be exceptionally brief ($\lesssim 10^3$ yr; Dwarkadas 2011). LBV stars are prime suspects because they undergo recurrent mass-loss episodes that eject large portions of their hydrogen envelope ($\gtrsim$ 1 $M_\odot$; Smith & Owocki 2006). However, traditional stellar evolutionary theory has predicted LBV stars to be a transitional phase lasting 10^4 to 10^5 yr before evolving to a compact and hydrogen-poor W-R star lasting a few $\times 10^5$ yr (Meynet et al. 1994; Langer et al. 1994; Maeder & Meynet 2000). This predicted timescale is discrepant with the $\sim$ 1 yr timescale between eruption and core collapse observed in at least some type IIn and Ibn systems (Pastorello et al. 2007, 2013; Smith et al. 2014).

The extent to which eruptive and/or accelerated mass loss may directly precede core collapse in a wider range of supernovae is poorly constrained, particularly in type IIb, Ib, and Ic supernovae (SN Ibc) where the progenitor star has been significantly stripped of its hydrogen enve-

[1] Harvard-Smithsonian Center for Astrophysics, 60 Garden Street, Cambridge, MA, 02138.
Electronic address: dmilisav@cfa.harvard.edu
[2] Department of Physics, University of Auckland, Private Bag 92019, Auckland, New Zealand
[3] Steward Observatory, University of Arizona, 933 N. Cherry Ave, Tucson, AZ 85721
[4] NASA Einstein Fellow
[5] Hartebeesthoek Radio Observatory, PO Box 443, Krugersdorp 1740, South Africa
[6] Department of Physics and Astronomy, York University, Toronto, ON M3J 1P3, Canada
[7] Astrophysical Institute, Department of Physics and Astronomy, 251B Clippinger Lab, Ohio University, Athens, OH 45701, USA
[8] Oskar Klein Centre, Department of Astronomy, Stockholm University, AlbaNova, SE106 91 Stockholm, Sweden
[9] Department of Physics & Astronomy, Dartmouth College, 6127 Wilder Lab, Hanover, NH 03755, USA
[10] Argelander-Institut f'ur Astronomie, Auf dem Hgel 71, 53121 Bonn, Germany

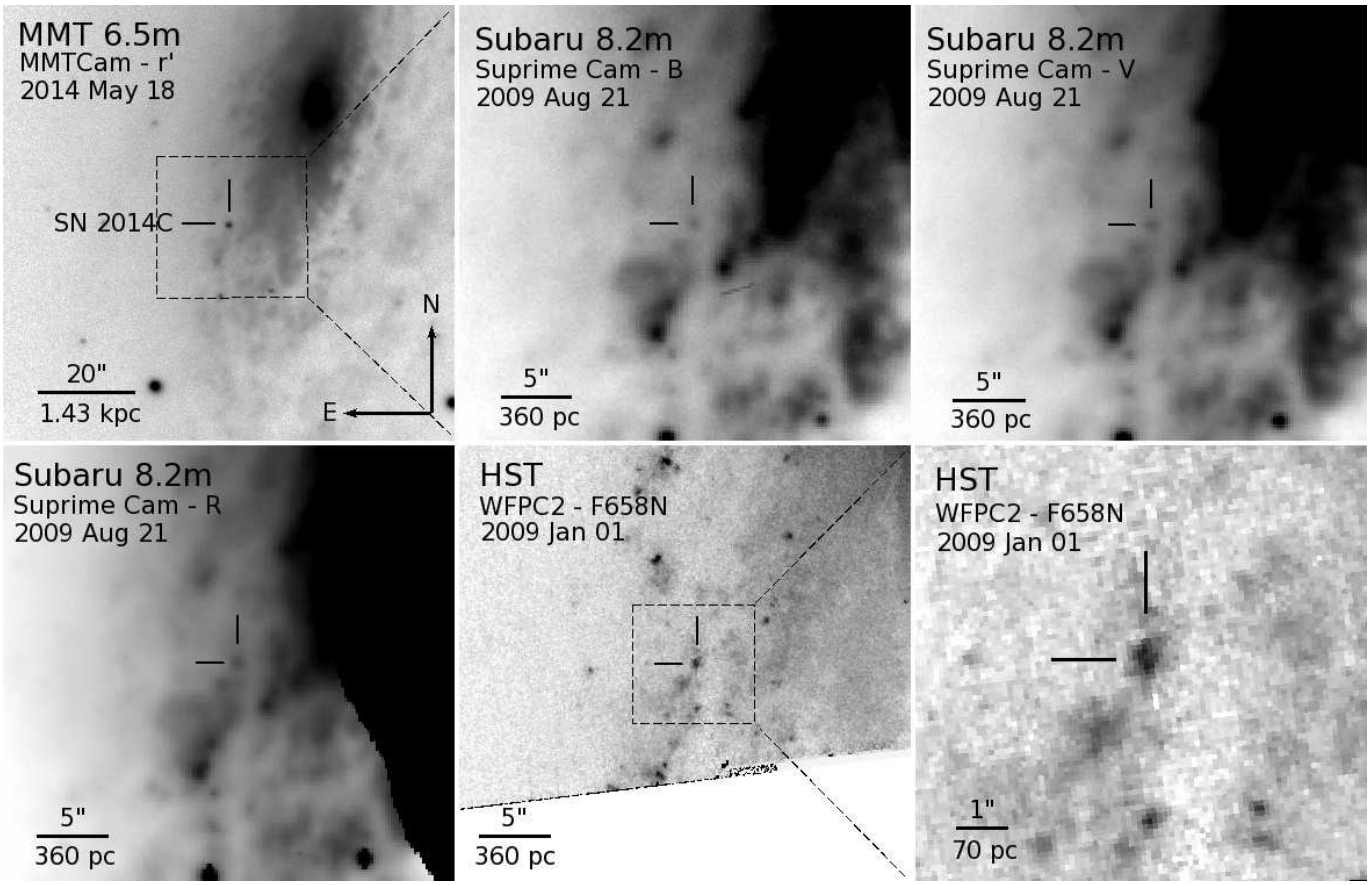

Figure 1. Finding chart of SN 2014C and pre-explosion images. Top left: MMT 6.5m telescope r'-band image of the region around SN 2014C (marked) and its host galaxy NGC 7331 obtained 2014 May 18 with the MMTCam instrument. Top middle and right and bottom left: Archival Subaru 8.3 m telescope BVR-band images obtained 2009 August 21 with the Suprime-Cam instrument. A visible source coincident with the location of the supernova is seen in all three filters. The galaxy nucleus in the R-band image is saturated and masks emission west of the supernova. Bottom middle and right: HST/WFPC2 F658N images. Dashed boxes outline enlarged regions shown in the adjoining panels.

lope. Some insight into this issue was provided by optical (Maeda et al. 2015) and radio+X-ray observations (Kamble et al. 2015) of the type IIb SN 2013df. Both studies concluded that the progenitor star experienced enhanced mass loss of $(3-8)\times10^{-5}\ M_{\odot}\ \mathrm{yr}^{-1}$ (for wind velocity of 10 km s^{-1}) in the final centuries leading up to the supernova explosion. Intriguingly, not all type IIb supernovae exhibit the same mass loss enhancement (e.g., SN 2011dh; Krauss et al. 2012; Maeda et al. 2014; de Witt et al. 2015). The underlying physical reasons for this dichotomy are presently unclear, but may be related to the progenitor star size and various channels of binary interaction (Maeda et al. 2015).

W-R stars have long been suggested as an obvious progenitor of SN Ibc because they are deficient in hydrogen (Gaskell et al. 1986). However, only progenitor stars with much cooler atmospheres than those of W-R stars have been unambiguously detected at the explosion sites of type IIb supernovae (Aldering et al. 1994; Maund et al. 2011; Van Dyk et al. 2014), and no secure direct identification has yet been made of a type Ib or Ic progenitor system (Van Dyk et al. 2003; Smartt 2009; Eldridge et al. 2013). A possible exception is the type Ib iPTF13bvn (Cao et al. 2013; Groh et al. 2013; Bersten et al. 2014; Eldridge et al. 2015; Fremling et al. 2014).

The observed number of W-R stars is probably insufficient to account for all SN Ibc, and low mass He stars in binary systems are more likely to be the dominant progenitor channel (Podsiadlowski et al. 1992; Wellstein & Langer 1999; Smartt 2009; Smith et al. 2011; Claeys et al. 2011; Langer 2012; Eldridge et al. 2013; Dessart et al. 2015; Eldridge et al. 2015). However, because W-R stars are difficult to detect in broad-band images and large populations may presently be unaccounted for (Shara et al. 2013; Massey et al. 2014, 2015), W-R stars may still represent a significant fraction of SN Ibc.

In this paper we present and analyze optical observations of a supernova that underwent a remarkable metamorphosis consistent with a delayed interaction between the core-collapse explosion and a massive circumstellar shell formed from the progenitor star's partially stripped hydrogen envelope. In Section 2, we present multi-epoch spectra of SN 2014C that follow its slow spectroscopic transformation from normal type Ib to strongly interacting type IIn, as well as archival pre-explosion images that show a luminous source coincident with the supernova. In Section 3, we discuss properties of the partially stripped progenitor star and its host environment, as well as possible physical mechanisms behind the formation of the circumstellar shell. Finally, in Section 4, we summarize our conclusions and outline how future work on late-interacting SN Ibc systems like SN 2014C can contribute

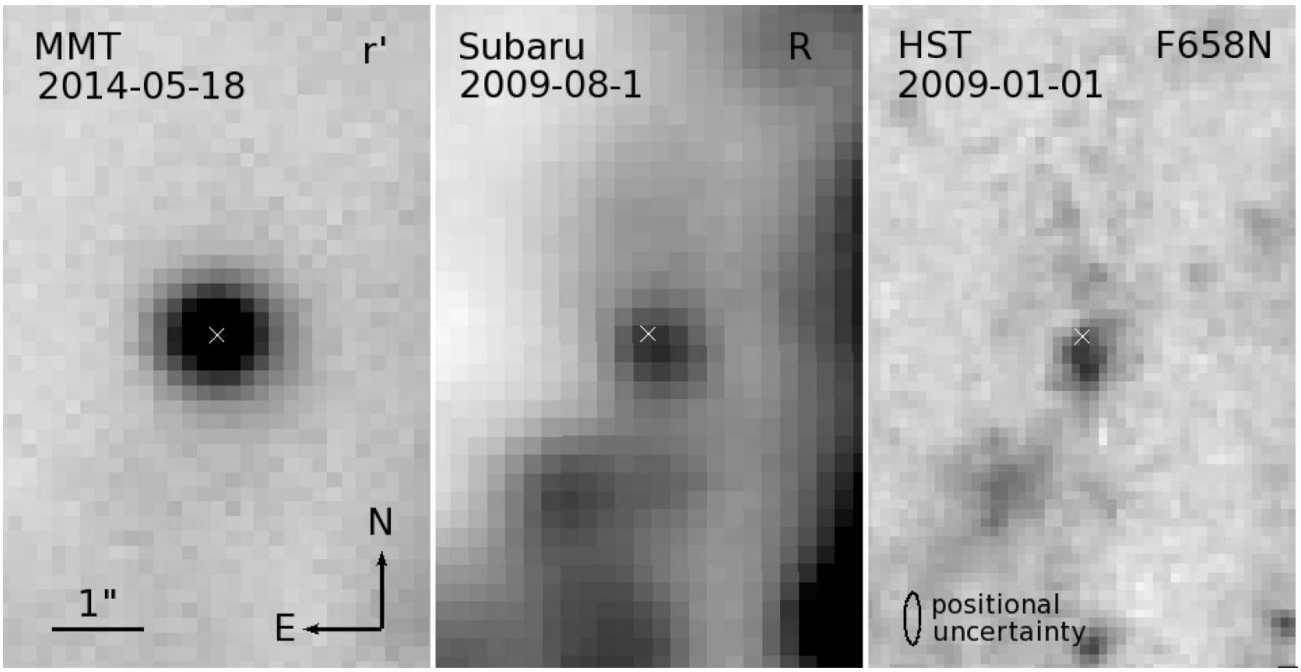

Figure 2. Enlarged images of SN 2014C and the coincident pre-explosion emission source. In all panels "X" marks the location of the best-fit centroid to the PSF of SN 2014C as determined from the MMTCam image. A 0.″24 offset is observed between the supernova centroid and the peak in emission of the coincident source observed in the Subaru images. The ellipse in the lower left corner of the bottom right panel is the 3σ error uncertainty in the alignment between the MMT and HST images.

unique information about poorly understood stages of stellar evolution and mass loss that immediately precede core collapse.

2. OBSERVATIONS AND RESULTS

SN 2014C was discovered at coordinates $\alpha = 22^{\rm h}37^{\rm m}05\overset{\rm s}{.}60$ and $\delta = +34°24'31\overset{''}{.}9$ (J2000.0) in the nearby spiral galaxy NGC 7331 on 2014 January 5.1 UT by the Lick Observatory Supernova Search (Kim et al. 2014). NGC 7331 is known to have hosted two previous supernovae: SN 1959D (Humason 1959) and SN 2013bu (Itagaki et al. 2013). In Figure 1, a finding chart for SN 2014C and its immediate environment made from an r'-band image obtained with the 6.5 m MMT telescope and the MMTCam instrument[11] is shown.

Shortly after the supernova's discovery, optical spectra obtained by J. Zhang & X. Wang with the 2.4m telescope of Yunnan Observatories and L. Tartaglia et al. with the Asiago 1.82m Copernico Telescope led to the classification of the supernova as a hydrogen-poor type Ib near maximum light. It was at this point that our group initiated a multi-wavelength (radio-to-X-ray) observing campaign. Optical/ultraviolet light curves and X-ray data are presented in Margutti et al. (2015), and radio data are presented in Kamble et al. (2015). Results from a search for pre-explosion images and optical spectroscopy during the first year of monitoring are presented here. Throughout this paper we adopt the Cepheid distance of 14.7 ± 0.6 Mpc to the host galaxy NGC 7331 (Freedman et al. 2001), and uncertainties are quoted at the 1σ confidence level (unless otherwise noted).

2.1. *Pre-Explosion Images*

NGC 7331 is an early type spiral galaxy that has been studied closely from X-ray to radio wavelengths (see, e.g., Thilker et al. 2007). Consequently, extensive archival data exist that cover the region of SN 2014C prior to explosion. We retrieved optical images originally obtained on 2009 August 21 with the 8.3 m Subaru Telescope and the Suprime-Cam instrument (Miyazaki et al. 2002), via the SMOKA Science Archive[12]. B, V, and R filters were used with exposure lengths of 200, 300, and 560 s, respectively. Images were bias-corrected and flat-fielded following standard procedures with the IRAF software[13], and the absolute positions were obtained using the `IMWCS` software[14] and the US Naval Observatory B-1.0 catalog (Monet et al. 2003).

We also retrieved archival Hubble Space Telescope (HST) images covering the location of SN 2014C from the Mikulski Archive for Space Telescopes. The images were obtained with the Wide Field Planetary Camera 2 (WFPC2) and the F658N filter ($\lambda_{\rm C} = 6591$ Å; $\delta\lambda = 29$ Å) on 2009 January 1 with a total integration time of 3×600 s under program 11966 (PI: Regan). We used the AstroDrizzle package of the DrizzlePac 2.0 software[15] to remove geometric distortion, correct for sky background variations, flag cosmic-rays, and drizzle the individual frames together.

A visible source is seen in close proximity with SN 2014C in all three filters of the Subaru images (Figure 1), as well as in the HST F658N image. The source in the Subaru images is unresolved, with a point spread function (PSF) that we fit with a Gaussian having a full

[11] http://www.cfa.harvard.edu/mmti/wfs.html

[12] http://smoka.nao.ac.jp/

[13] The Image Reduction and Analysis Facility is distributed by the National Optical Astronomy Observatories, which are operated by the Association of Universities for Research in Astronomy, Inc., under cooperative agreement with the National Science Foundation.

[14] http://tdc-www.harvard.edu/wcstools/

[15] http://drizzlepac.stsci.edu/

Table 1
Log of spectroscopic observations

Date	MJD	Phase (days)	Telescope	Instrument	Grating	Range (Å)	Resolution (Å)
2014 Jan 09	56666.08	-4	FLWO	FAST	300	3500 − 7400	7.0
2014 May 06	56783.43	113	MMT	Blue Channel	300	3300 − 8500	7.0
2014 Oct 22	56953.28	282	LBT	MODS	Dual	5000 − 10000	3.0
2015 Jan 21	57043.08	373	MMT	Blue Channel	300	3500 − 8500	7.0
2015 Apr 25	57137.47	467	MMT	Blue Channel	1200	4270 − 5300	1.5

* Phase is with respect to estimated V-band maximum on 2014 January 13 (MJD 56670) reported in Margutti et al. (2015).

width at half maximum (FWHM) comparable to that observed in nearby stars ($\approx 0\farcs8$; average of five stars). The source seen in the HST image is resolved, non-uniform and extended in distribution. It is slightly elongated in the north-south direction and is contained within an approximate effective radius of $\approx 0\farcs24$.

We used the `GEOMAP` task of IRAF to determine a spatial transformation function between the MMT, Subaru, and HST images, and the `GEOTRAN` task to apply the transformation. Figure 2 shows the location of the pre-explosion sources with respect to SN 2014C as observed in the MMT image. A small offset of $0\farcs24 \pm 0.05$ exists between the centroid of SN 2014C observed in the MMT image and the emission peak of the source observed in the Subaru image. A small offset is also seen between the location of SN 2014C and the approximate center of the extended region observed in the HST F658N image.

We performed PSF photometry on the Subaru images using the `DAOPHOT` package in IRAF in order to constrain emission properties of the potential progenitor system. The images were calibrated via relative photometry using 10 stars in Sloan Digital Sky Survey (SDSS) images that cover the field of view. Photometric transformations were made from Jordi et al. (2006) to put SDSS photometry into the $BVRI$ system. The apparent magnitudes of the coincident source are $m_B = 22.18 \pm 0.13$, $m_V = 21.13 \pm 0.09$, and $m_R = 20.28 \pm 0.06$. The region surrounding the source has considerable galaxy light and the reported apparent magnitudes may overestimate the brightness. The uncertainties reflect the error in PSF fitting and do not include possible error due to contamination from galaxy light.

We measured the flux contained within a $0\farcs5$ aperture centered on the coincident emission source observed in the HST/WFPC2 F658N image. The sum count rate 1.00 ± 0.01 counts s^{-1} was multiplied by the modified PHOTFLAM parameter (9.87×10^{-17} erg s^{-1} cm^{-2} Å^{-1}) and the effective bandpass of the filter given by the RECTW parameter (39.232 Å). The integrated flux, which is a sum of narrow Hα, [N II] $\lambda\lambda$6548, 6583, and continuum emission, is $(3.87 \pm 0.04) \times 10^{-15}$ erg s^{-1} cm^{-2}. By estimating the contribution from continuum emission from the spectral energy distribution (SED) of the Subaru photometry, and assuming the contribution from the [N II] lines to be $\approx$ 0.13 per cent of the continuum subtracted flux, we derive an observed Hα flux of 2.9×10^{-15} erg s^{-1} cm^{-2}, and an unabsorbed luminosity of 4.3×10^{38} erg s^{-1} after correcting for $E(B-V)_{\rm total}$ (cf. Section 2.2).

2.2. *Optical Spectroscopy*

Low-resolution optical spectra of SN 2014C were obtained from three telescopes: The F. L. Whipple Observatory (FLWO) 1.5 m Tillinghast telescope mounted with the FAST instrument (Fabricant et al. 1998), the 6.5 m MMT Telescope mounted with the Blue Channel instrument (Schmidt et al. 1989), and the 2×8.4 m Large Binocular Telescope mounted with the MODS instrument (Pogge et al. 2010). Details of the observations are provided in Table 1.

Our five epochs of optical spectra of SN 2014C are plotted in Figure 3. The explosion date is not tightly constrained by the light curve, so we use the peak in the V-band on 2014 January 13 as the reference from which phase in days is measured (Margutti et al. 2015).

Standard procedures to bias-correct, flat-field, and flux calibrate the data were followed using the IRAF/PYRAF software[16] and our own IDL routines. A recession velocity of 990 km s^{-1}, determined from many narrow emission lines including [O III] $\lambda\lambda$4959, 5007, Hα, and [S II] $\lambda\lambda$6716, 6731, was removed from all spectra. Line identifications and estimates of expansion velocities of the photospheric spectra were made with the supernova spectrum synthesis code `SYN++` (Thomas et al. 2011). Narrow emission line identifications in late-time spectra were made using lists provided in Fesen & Hurford (1996).

The foreground extinction due to the Milky Way is $E(B-V)_{mw} = 0.08$ mag (Schlafly & Finkbeiner 2011). The host internal extinction was estimated by measuring the equivalent width (EW) of Na I D absorption in our optical spectra and following the prescriptions of Turatto et al. (2003). The EW(NaID) from the day -4 spectrum is 4.25 ± 0.07 Å. Using the lower branch of the Turatto et al. (2003) relation (see their Fig. 3), this measurement of EW(Na I) implies $E(B-V)_{\rm host} = 0.67 \pm 0.01$ mag. We adopted a total extinction of $E(B-V)_{\rm total} = 0.75 \pm 0.08$ mag, which combines the Galactic extinction with the inferred host extinction. We confirmed that this extinction estimate provides an appropriate $(B-V)$ color correction to the color indices of SN 2014C to match those of other type Ib supernovae (Margutti et al. 2015). All extinction corrections made in this paper use $E(B-V)_{\rm total}$, in combination with the standard reddening law of Cardelli et al. (1989) assuming $R_{\rm V} = 3.1$.

2.3. *Spectroscopic Metamorphosis*

Our optical spectrum obtained 2014 January 09 (day -4) shows features clearly associated with Fe II, He I, Ca II, exhibiting velocities of $(1.3 \pm 0.1) \times 10^4$ km s^{-1}

[16] PYRAF is a product of the Space Telescope Science Institute, which is operated by AURA for NASA.

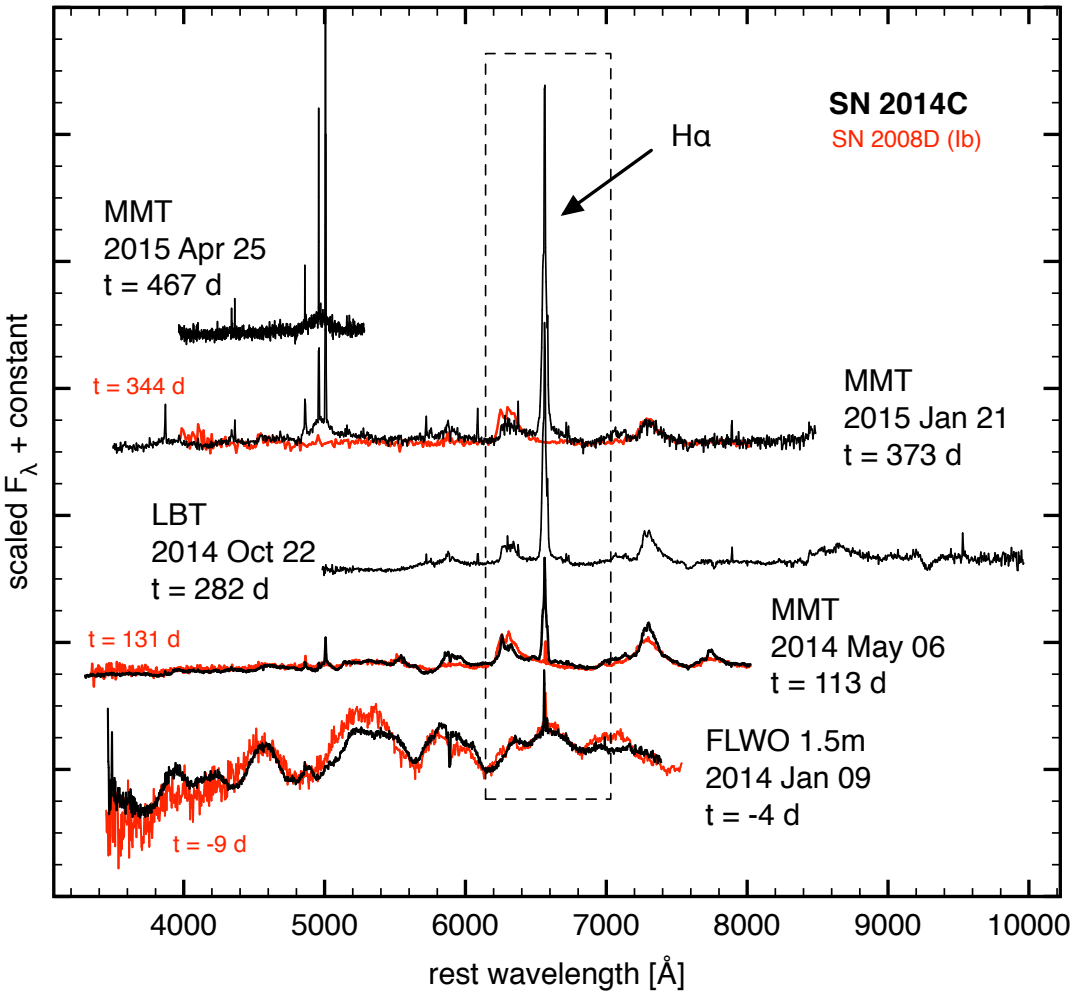

Figure 3. Five epochs of optical spectra of SN 2014C. Telescopes used, dates of observations, and phases with respect to V-band maximum on 2014 January 13 are provided. Three epochs of spectra of the H-poor type Ib SN 2008D, originally published in Modjaz et al. (2009) and Tanaka et al. (2009), are shown for comparison. Epochs for SN 2008D are with respect to V-band maximum on 2008 January 28 (Modjaz et al. 2009). At maximum light, SN 2014C exhibits a spectrum very similar to that of SN 2008D. One year later, however, the spectrum of SN 2014C is largely dominated by Hα with a profile having an extended FWHM width of ≈ 1400 km s^{-1} that is normally only observed in H-rich type IIn supernovae. Refer to Figure 6 for an enlargement of the day 373 spectrum.

(Figure 4). These are features regularly seen in type Ib supernovae (Filippenko 1997), including well-known examples SN 2008D (Modjaz et al. 2009) and iPTF13bvn (Srivastav et al. 2014). An absorption centered around 6150 Å is typically associated with Si II, however we find that the spectrum is best fit with a combination of high velocity (HV) Hα features spanning $(1.3-2.1)\times 10^4$ km s^{-1}. This choice of line identification is discussed in greater detail in Section 3.2.

Follow-up spectroscopic observations did not resume until day 113 when the supernova returned from behind the Sun. Interestingly, the day 113 spectrum of SN 2014C exhibits a mix of standard and non-standard emissions. The broad [O I] $\lambda\lambda$ 6300, 6364 and [Ca II] $\lambda\lambda$7291, 7324 emission observed in the spectrum are a normal feature of type Ib supernovae several months after explosion and are associated with inner metal-rich ejecta that are radioactively heated by ^{56}Co. Most unusual, however, was conspicuous emission centered around the Hα line with an overall FWHM of 1400 km s^{-1} that had emerged. This emission continued to grow in strength relative to other emission lines over the next several months (Figure 3).

An extraordinary event must have occurred while SN 2014C was hidden behind the Sun. An intermediate-width Hα feature is normally seen only in type IIn supernovae, where it is associated with radiative shocks in dense clouds (Chugai & Danziger 1994). The interaction decelerates the blast wave and a dense shell traveling approximately at the shock velocity is formed. Accordingly, we interpret the conspicuous change in Hα emission from SN 2014C to be the result of the supernova having encountered dense H-rich circumstellar material (CSM) between Februrary and May 2014. Consistent with this scenario (see, e.g., Chevalier & Fransson 2006), strong radio and X-ray emission accompanied the sudden increase in Hα emission in SN 2014C as the shock continued to strongly interact with the density spike in CSM (Margutti et al. 2015; Kamble et al. 2015).

We attempted to decompose the complex line profile centered on Hα in the spectra into multiple Gaussian features. After removing the linear continuum and running a least-squares fitting routine, we found that the profile could be reasonably reproduced with narrow components

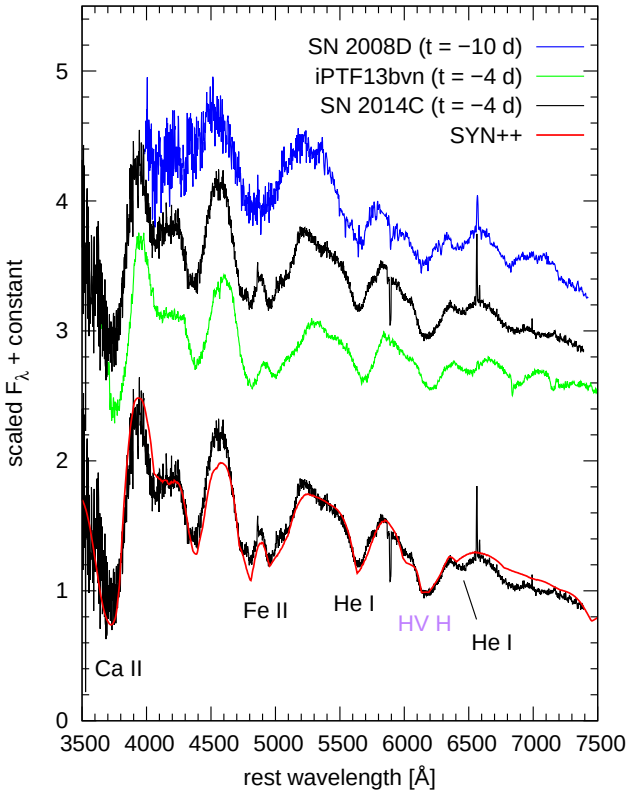

Figure 4. The spectrum of SN 2014C compared to those of other type Ib supernovae near maximum light. The spectra of SN 2014C and SN 2008D have been corrected for extinction using $E(B-V)$ values of 0.75 mag (this paper) and 0.5 mag (Soderberg et al. 2008; Modjaz et al. 2009), respectively, whereas the spectrum of iPTF13bvn has not been corrected (Cao et al. 2013; Srivastav et al. 2014). The data were originally published in Modjaz et al. (2009) and Srivastav et al. (2014) and were digitally retrieved from WISEREP (Yaron & Gal-Yam 2012). Also shown is a synthetic spectrum of SN 2014C created with `SYN++`. Some absorption features dominated by single ions with projected Doppler expansion velocities of $(1.3 \pm 0.1) \times 10^4$ km s^{-1} are identified, as well as high velocity (HV) hydrogen that spans $(1.3 - 2.1) \times 10^4$ km s^{-1}.

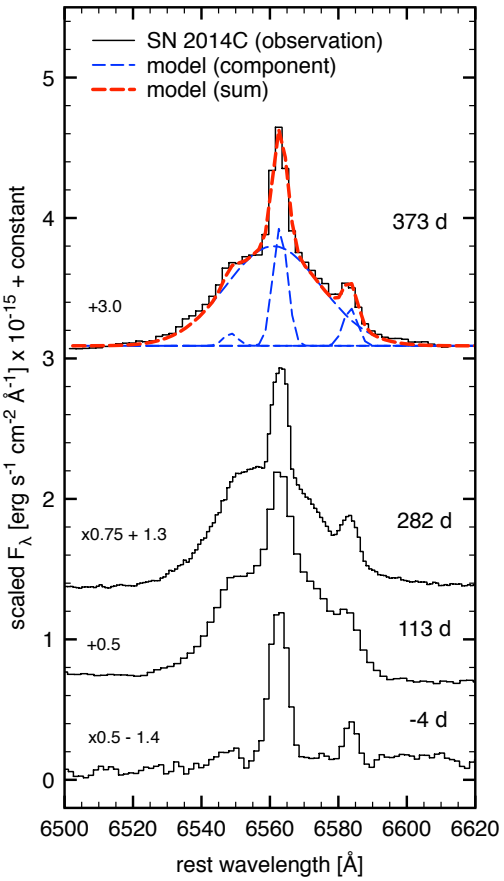

Figure 5. Evolution of the emission line profile around Hα. On day −4 only unresolved (FWHM $\approx$ 250 km s^{-1}) Hα and [N II] $\lambda\lambda$6548, 6583 lines are observed. Subsequently, beginning on day 113, an intermediate component (FWHM $\approx$ 1200 km s^{-1}) is observed. A model fitting the day 373 profile is shown. Scaling parameters are given to the left of each spectrum.

of Hα and [N II] 6548, 6583 lines having instrumentally unresolved FWHM velocities of $\approx$ 250 km s^{-1} and an intermediate-width component with a FWHM width of 1200 ± 100 km s^{-1} (Figure 5). The Hα profile extends to 6520 Å and 6610 Å, which sets limits on the velocity of the emitting shocked CSM to −2000 and +2200 km s^{-1}. The narrow components are presumably associated with wind material that is being photoionized by X-rays of the forward shock, and the intermediate component is associated with the shock and/or ejecta running into CSM. The day −4 spectrum, which has only narrow components, is most likely a combination of emission local to the supernova and from the entire host massive star cluster (see Section 2.1). We interpret emission at later epochs to be be dominated by emission from supernova-CSM interaction.

Beginning with the day 282 spectrum and continuing with the day 373 spectrum, the emissions are increasingly complex and originate from several distinct regions. Figure 6 shows an enlargement of the day 373 spectrum corrected for extinction and a complete list of identified emission features. Several narrow, unresolved emission lines are observed including [O III] λ4363 and $\lambda\lambda$4959, 5007, [Ne III] λ3869, He II λ4686, and [N II] λ5755. Also seen are several narrow, unresolved coronal lines including [Fe VI], [Fe VII], [Fe X], [Fe XI], and [Fe XIV]. We attribute this emission to ionization of the pre-shock circumstellar gas by X-rays emitted by the shocked gas. The strongest constraint on the wind velocity comes from the day 474 spectrum that has the highest resolution of all our data. We measure a FWHM width of 1.5 Å (which is unresolved) in the [O III] λ4363 emission line. This sets an upper limit of < 100 km s^{-1} for the unshocked wind velocity.

Broad emission centered around the [O III] $\lambda\lambda$4959, 5007 lines is seen in our spectra beginning on day 282 and continues to be visible through our last spectrum obtained on day 474. The width of the emission is difficult to measure since it blends with Hβ blueward of 4959 Å and another source of emission redward of 5070 Å. We estimate that the velocity width must be $\gtrsim 3500$ km s^{-1}, meaning that the emission originates from a region different than the shocked CSM. Presumably it is emission from oxygen-rich stellar ejecta being excited by the reverse shock. Broad [O III] emission is normally only seen in supernovae many years to decades after core collapse (Milisavljevic et al. 2012). But in the case of SN 2014C, the supernova-CSM interaction may have accelerated its

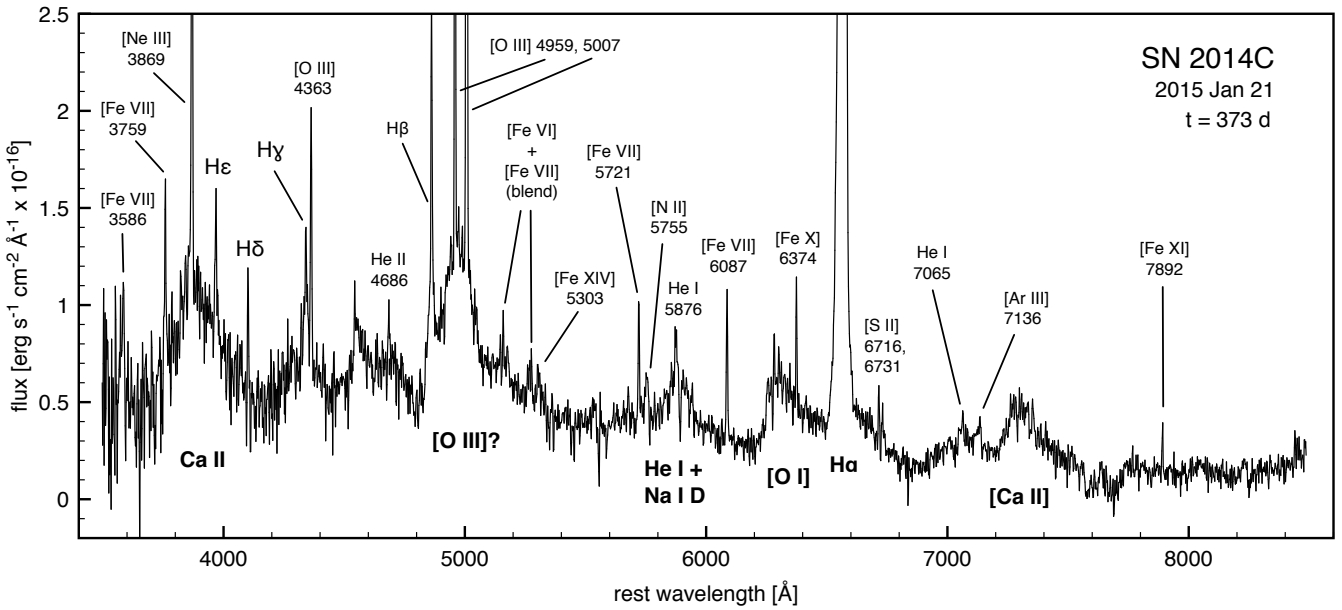

Figure 6. Dereddened MMT spectrum of SN 2014C. The emission arises from various regions of shocked and photoionized CSM and stellar ejecta. Broad components are identified in bold below the spectrum, and narrow components are identified above the spectrum.

dynamical evolution.

By comparing the overall emission profile around 7300 Å to that observed around [O I] $\lambda\lambda$6300, 6364, we find that the velocity distribution is best matched when measured with respect to the [Ca II] $\lambda\lambda$7291, 7324 lines (λ_C =7307 Å) as opposed to the [O II] $\lambda\lambda$7319, 7330 lines (λ_C =7325 Å). Detecting emission from [O I] and [Ca II], but not from [O II], implies that the ejecta associated with this emission have densities that are $\gtrsim 10^6$ cm^{-3} (Fesen et al. 1999).

The dereddened day 373 optical spectrum exhibits a blue pseudo-continuum, which is sometimes seen in type IIn and Ibn supernovae and has been attributed to fluorescence from a number of blended emission lines (Fransson et al. 2002; Foley et al. 2007; Smith et al. 2009; Figure 7). One of the strongest expected fluorescence-pumped Fe II lines is at 8451 Å (Fransson et al. 2002). Near this wavelength region we detect a minor emission peak centered at 8446 Å in our day 282 spectrum that is blended with the Ca II near-infrared triplet. This feature is most likely the O I recombination line at 8446 Å and not Fe II. We also do not observe Fe II lines at 9071, 9128, or 9177 Å, which would be expected to accompany the Fe II λ8451 line (Fransson et al. 2002).

2.4. *Properties of the unshocked CSM*

Properties of the surrounding unshocked CSM shed from the progenitor star of SN 2014C can be estimated using the relative line strengths of narrow features observed in our optical spectra. The forbidden oxygen lines provide a lower limit to the density. We do not detect narrow [O II] λ3727, but we do detect [O III] $\lambda\lambda$4959, 5007, indicating that electron densities are well above 10^4 cm^{-3} in this emitting region (Osterbrock & Ferland 2006). An upper limit to the density can be estimated from the relative line strengths of [Fe VII]. Comparing these line strengths with the CHIANTI database (Landi et al. 2013), we find that the density is less than 10^7 cm^{-3}. An estimate of the temperature can be derived using the [O III] line diagnostic $R = \lambda(4959{+}5007)/\lambda4363$ for densities between $10^5 - 10^6$ cm^{-3} using the `TEMDEN` task in IRAF (Shaw & Dufour 1994). We measure $R = 9.8{\pm}0.2$, which is associated with temperatures between $(2-8)\times10^4$ K.

The ratio of [N II] λ6583 / H$\alpha \approx 0.3$ in the day 373 spectrum is higher than the ratio observed in the day -4 spectrum (i.e., before interaction commenced) where it is ≈ 0.15. An increase in temperature, which would be anticipated from the hard ionizing spectrum and high density that suppresses some of the forbidden line cooling, may explain the high ratio. The increase could also be indicative of nitrogen-enriched CSM from CNO processing in the progenitor star.

Knowledge of the X-ray luminosity L_x around day 373 can further constrain properties of the unshocked CSM. The ionization parameter is defined as

$$\xi = L_x/(nr^2), \tag{1}$$

where n is the electron density number, and r is the radius of the emitting region. L_x at this time is $\sim 5{\times}10^{40}$ erg s^{-1} and consistent with a temperature of 18 keV (Margutti et al. 2015). Kallman & McCray (1982) find that the Fe VII ion fraction peaks at about 30% for $\xi \sim 10$ in models with photoionizing 10 keV bremsstrahlung spectra that are expected to be at least approximately applicable to SN 2014C. Thus,

$$nr^2 = L_x/\xi \sim 5\times10^{39}\ \mathrm{cm}^{-1} \tag{2}$$

Although there must be a range of ionization parameters present, the ratio of [Fe XIV] λ5303/[Fe X] λ6374 is only 0.18 ± 0.03, which indicates that ξ only goes up to ≈ 25.

The emission measure EM is defined as

$$\begin{aligned} EM &= (4\pi/3)n^2r^3f \\ &= \frac{L_{[\mathrm{Fe\ VII}]}f}{j_\epsilon A_{(Fe)}\eta} \end{aligned} \tag{3}$$

where j_ϵ is the emissivity, $A_{(Fe)}$ is the Fe abundance (2.75×10^{-5}), η is the ion fraction, and f is the filling factor. We measure the line flux of [Fe VII] λ6087 to be $5.2{\times}10^{-15}$ erg cm^{-2} s^{-1}, which translates to a luminosity of $1.4{\times}10^{38}$ erg s^{-1}. The emissivity for the [Fe VII] λ6087 line from CHIANTI is 1.3×10^{-20} erg s^{-1} cm^{-3} sr^{-1}.

Solving equation (3) for r in terms of equation (2),

$$r = \frac{(nr^2)^2}{EM(4\pi/3)f}, \tag{4}$$

yields a radius of $4.9 \times 10^{15}\ f^{-1}$ cm. Recasting equation (2) in terms of n, and substituting this value of r we find that

$$n = L_x/(\xi r^2) \sim 2 \times 10^8\ f^2\ \mathrm{cm}^{-3}. \tag{5}$$

With the constraint that $n \lesssim 10^6$ cm^{-3} from the forbidden oxygen and iron line diagnostics, equation (5) implies that $f \lesssim 0.1$, which is reasonable since the gas that contributes to the highest-ionization Fe lines may fill only some of the volume. The temperatures, densities, and filling factor we derive suggest that the emission is not uniformly distributed and originates from clumped material. A full treatment of emission line modeling is left for future work.

3. DISCUSSION

SN 2014C represents the first time an ordinary type Ib supernova has been seen to slowly evolve into a strongly interacting type IIn. This Ib-IIn metamorphosis is consistent with a delayed interaction between an H-poor star's supernova explosion and a local H-rich shell presumably formed from material stripped from the progenitor star. The strong supernova-CSM interaction must have started between February and May of 2014 while the supernova was behind the Sun. Type Ib supernovae have typical rise times of $\lesssim$ 20 days (Drout et al. 2011; Bianco et al. 2014), thus the strong interaction occurred somewhere between $\approx$ 20 and 130 days after explosion. Assuming a minimum forward shock velocity of $0.1\,c$, we can loosely constrain the radius of the shell to be $\gtrsim 3 \times 10^{16}$ cm from the explosion center.

In Figure 7, SN 2014C is compared to two representative objects: the type IIn SN 2005ip (Stritzinger et al. 2012) and the type Ibn SN 2006jc (Modjaz et al. 2014). Spectroscopic differences and similarities between these supernovae reflect the distance of the CSM shell with respect to the explosion and the shell's chemical composition. In type IIn and Ibn supernovae, massive and dense CSM is located nearby and interaction commences shortly ($\lesssim$ 1 day) after explosion. Consequently, an opaque CSM hides the interior and O-rich material is often never observed. This contrasts with SN 2014C, where the longer delay between explosion and interaction is associated with a larger, less dense and less opaque shell. This latter situation is advantageous as it permits observations of interior processes that are normally hidden.

3.1. *Previous examples of delayed interaction*

The closest analog to SN 2014C in overall properties is SN 2001em. That supernova was spectroscopically classified as a hydrogen deficient type Ib/c (Filippenko & Chornock 2001)[17], two years before it was re-detected as a highly luminous radio source (Stockdale et al. 2004), and showed intermediate-width Hα emission with FWHM $\sim$ 1800 km s^{-1} in its optical spectra (Soderberg et al. 2004). Unlike SN 2014C, the intermediate stages between H-deficient to H-dominated emission in SN 2001em was completely missed.

Although it was originally thought that SN 2001em may harbor a bipolar relativistic off-axis jet that had decelerated to mildly relativistic velocities (Granot & Ramirez-Ruiz 2004), later observations with very long baseline interferometry ruled this model out by demonstrating that the expansion velocity of the supernova was below 6000 km s^{-1} and that the supernova was therefore not driven by a relativistic jet (Bietenholz & Bartel 2005, 2007; Schinzel et al. 2009). Chugai & Chevalier (2006) found that the multi-wavelength properties of SN 2001em could be modeled in a scenario in which non-relativistic ejecta from the supernova explosion collided with a dense and massive ($\sim$ 3 $M_\odot$) circumstellar shell at a distance of $\sim 7 \times 10^{16}$ cm from the star. The circumstellar shell was presumably formed by a vigorous mass loss episode with a mass loss rate of $\sim 2 \times 10^{-3}$ M$_\odot$ yr^{-1} approximately 1000 to 2000 yr prior to the supernova explosion. The hydrogen envelope was completely lost and subsequently swept up by the fast wind of the pre-supernova star and accelerated to a velocity of 30-50 km s^{-1}. Such a high-rate mass-loss event could be explained by binary interaction, but could also be explained by a powerful eruption from an LBV star. A similar scenario is possible for SN 2014C, but in this case, less of the progenitor's H-rich envelope had been stripped at the time of explosion (see additional discussion in section 3.4).

Late-time interaction with dense CSM shells has been observed in a handful of supernovae with H-rich ejecta. For example, the progenitor of SN 1996cr evacuated a large cavity just prior to exploding, and the forward blast wave likely spent 1-2 yr in relatively uninhibited expansion before eventually striking a dense shell of CSM (Bauer et al. 2008). SN 1996cr may be a "wild cousin" of SN 1987A, which has slowly interacted with a dense ring at a radius of 6×10^{17} cm (approximately an order of magnitude larger than the shell radius inferred for SN 2014C) beginning as early as 1995 (Sonneborn et al. 1998; Lawrence et al. 2000).

3.2. *Partially stripped progenitor star*

Our modeling of the near-maximum light optical spectrum of SN 2014C associates absorption around 6150 Å with high velocity hydrogen (Figure 3). Attempts to model the 6150 Å absorption with Si II were unsuccessful because the velocity as inferred from the minimum of the feature ($v \approx 8000$ km s^{-1}) was inconsistent with those inferred from all other ions ($v \approx 13000$ km s^{-1}, cf. Section 2.3). Alternative identifications for this absorption feature that have been investigated elsewhere for other SN Ibc, including C II and Ne I (Harkness et al. 1987;

[17] The text of Filippenko & Chornock (2001) reads "type Ib or Ic (most likely Ic), perhaps a month after maximum brightness." We visually inspected these data published in van Dyk (2010) and agree with their classification.

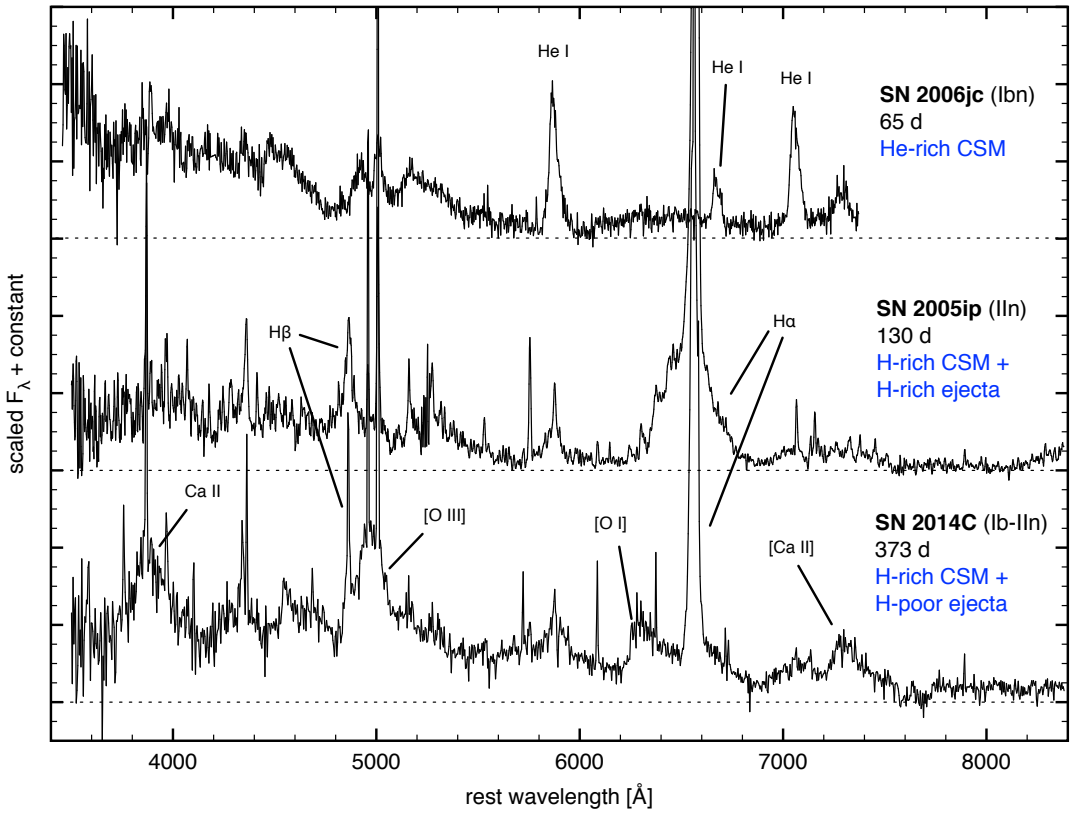

Figure 7. Dereddened MMT spectrum of SN 2014C compared to the spectra of the type IIn SN 2005ip (Stritzinger et al. 2012) and the type Ibn SN 2006jc (Modjaz et al. 2014) retrieved from WISEREP. Prominent emission features associated with excited CSM and supernova ejecta are highlighted. Type IIn supernovae exhibit complex H Balmer profiles that are a blend of broad (> 5000 km s^{-1}), intermediate (~ 1000 km s^{-1}) and narrow (< 200 km s^{-1}) velocity components associated with H-rich ejecta, supernova-CSM interaction, and photoionized CSM, respectively. Type Ibn supernovae exhibit prominent intermediate width He I emission from supernova-CSM interaction and no emission from interior ejecta. SN 2014C exhibits intermediate width Hα and emission from interior O-rich material excited by radioactive decay of ^{56}Co. Many narrow lines associated with photoionized wind material are shared between all three supernovae. Dashed horizontal lines provide a baseline to compare increases in continuum strength toward shorter wavelengths.

Deng et al. 2000), were ruled out as strong contributors in SN 2014C. Our model is consistent with recent work by Parrent et al. (2015), who find that Si II is unlikely to be the dominant contributor to the absorption feature near 6150 Å seen in many SN Ibc.

The detection of hydrogen absorption around the time of maximum light implies that the progenitor star of SN 2014C was only partially stripped of hydrogen at the time of explosion. This is an important observation because it informs about the evolutionary status of the star at the time of core collapse. It is also relevant for debates on the extent of H and He in SN Ibc (Matheson et al. 2001; Branch et al. 2002, 2006; Hachinger et al. 2012; Milisavljevic et al. 2013; Modjaz et al. 2014; Milisavljevic et al. 2015; Parrent et al. 2015). The range of projected Doppler velocities used in fitting the optical spectrum with H I ($1.3 - 2.1 \times 10^4$ km s^{-1}) is consistent with a detached envelope consisting of an extended layer of hydrogen beyond the otherwise fairly sharp photosphere. It is beyond the scope of this paper to accurately estimate the mass of hydrogen associated with the detached envelope, but the models of Hachinger et al. (2012) provide useful upper limits. Hachinger et al. conclude that $\approx 0.03\ M_\odot$ of hydrogen is sufficient for Hα absorption to dominate over absorption due to Si II λ6355, as it does in SN 2014C.

Mass loss in massive stars is correlated with metallicity (Vink et al. 2001; Vink & de Koter 2005). The oxygen abundance of the explosion site of SN 2014C measured from our day -4 spectrum using the $N2$ scale of Pettini & Pagel (2004) is $\log(\mathrm{O/H}) + 12 = 8.6 \pm 0.1$, which is near the solar value ($\log(\mathrm{O/H})_\odot + 12 = 8.69$; Asplund et al. 2005). Our measurement is consistent with an independent measurement of the oxygen abundance of the center of NGC 7331 ($\log(\mathrm{O/H}) + 12 = 8.75 \pm 0.18$; Gusev et al. 2012). The explosion site metallicity of SN 2014C is above the median metallicity of type Ib supernovae with secure classifications, which is $\log(\mathrm{O/H})_\odot + 12 = 8.43 \pm 0.14$ (Sanders et al. 2012), and in line with the mean metallicity of type IIn, which is $\log(\mathrm{O/H})_\odot + 12 = 8.63 \pm 0.03$ (Taddia et al. 2015) (both measured with the same $N2$ scale). However, the explosion site metallicity is consistent with the metallicity distribution observed for each class, which are largely overlapping. SN 2014C was discovered in a targeted survey, which is known to favor the discovery of supernovae in brighter and more metal-rich galaxies (Sanders et al. 2012).

3.3. *Pre-explosion detection of progenitor system*

Valuable information about the progenitor system comes from the Subaru and HST pre-explosion imaging (Figures 1 and 2). Correcting for extinction using $E(B-V)_{\mathrm{total}}$, the absolute magnitude of the coincident

source is $M_V = -12.0 \pm 0.17$ mag. The luminosity rivals that of the most luminous stars known, suggesting that the source is not a single star and is instead a massive star cluster. Supporting this conclusion are the facts that 1) the source is extended and composite in the HST F658N image with an effective radius of ≈ 17 pc (cf. Section 2.1) that is consistent with observed sizes of massive star clusters (see, e.g., Bastian et al. 2013), and 2) SN 2014C has a noticeable offset from the center of the source (Fig. 1).

We compared the photometry and estimate of Hα luminosity of the pre-explosion source to the Binary Population and Spectral Synthesis (BPASS) stellar population models (Eldridge & Stanway 2009; Eldridge et al., in preparation; http://bpass.auckland.ac.nz). Assuming the total extinction $E(B-V)_{\rm total}$, we find that the best fitting age of the stellar population is between 30 to 300 Myr. The detection of Hα emission from the pre-explosion source favors younger populations closer to 30 Myr, and binary star models match estimates derived from the Hα luminosity more closely than those derived from single star models. The turn off mass of stellar populations in the favored age range is between 3.5 to 9.5 $M_\odot$, and the mass of the cluster is estimated to be between 3×10^5 and $10^6 M_\odot$. These age constraints are the same for three metallicities close to that of the environment of $Z = 0.008$, 0.014 and 0.020, where solar metallicity is between 0.014 and 0.020.

A source of uncertainty in our analysis of the host massive star cluster is in our estimate of the foreground extinction. It is unknown whether the extinction estimated from the day -4 optical spectrum of SN 2014C is local to the supernova, or along the line of sight to the entire cluster. An additional complication is that if the extinction is local, then it is possible that the extinction may have changed with time. Thus, within the stated uncertainties, the uncorrected absolute magnitudes represent lower limits to the luminosity of the cluster.

3.4. *Origin of the CSM shell*

Massive stars are known to become stripped of their outer layers in a variety of ways including line-driven winds and binary interactions (Podsiadlowski et al. 1992; Woosley et al. 1995; Wellstein et al. 2001; Vink et al. 2001; Puls et al. 2008; Yoon et al. 2010), but the details behind the precise physical mechanisms that are involved and the stages that this mass loss takes place are not well constrained (see Eldridge et al. 2008; Langer 2012; Smith 2014 and references therein). Any plausible explanation of the origin of the dense CSM shell with which SN 2014C interacted must be able to account for two key properties of the system. One property is the distance of the shell from the progenitor star of SN 2014C, which is much more distant than the shells in the majority of type IIn and Ibn supernovae. Another property is that the progenitor star exploded as a type Ib supernova, meaning that it had been largely stripped of its hydrogen envelope at the time of core collapse.

Below, we discuss three plausible scenarios for the physical origin of the massive shell that surrounded SN 2014C at the time of explosion.

3.4.1. *An unusually short W-R phase*

W-R stars have significant stellar winds, with mass loss rates of a few times $10^{-5} M_\odot$ yr^{-1} and terminal wind velocities of $1000 - 3000$ km s^{-1}(Crowther 2007). These winds can run into and overtake the much slower winds (< 100 km s^{-1}) of a previous red supergiant (RSG) phase and create massive CSM shells, or "bubbles," (see, e.g., Garcia-Segura et al. 1996). Approximately half of the Galactic population of W-R stars are associated with a CSM shell, some of which have anomalous abundances associated with ejected CNO-processed stellar material (Miller & Chu 1993). However, the majority of these CSM shells have diameters of many parsecs, which is much larger than the radius of the shell inferred for SN 2014C (~ 0.01 pc). Thus, SN 2014C did not interact with an environment like those typically observed around W-R stars.

However, it is possible that the progenitor star of SN 2014C evolved through a brief W-R phase lasting much less than 10^4 yr. Although traditionally it has been believed that massive stars should spend $0.5 - 1$ Myr in the core-He-burning W-R phase before finally exploding as normal SN Ibc (Heger et al. 2003), advances in stellar evolution modeling show many pathways that may potentially lead to short-lived W-R stars. Examples include low mass binary stars (Eldridge et al. 2008), and RSGs with strong pulsation-driven superwinds (Yoon & Cantiello 2010). Analyses of circumstellar environments around supernova remnants also support the notion that progenitors of stripped-envelope supernovae may pass through brief W-R phases (Schure et al. 2008; Hwang & Laming 2009).

However, a short W-R phase associated with a typical mass loss rate of a few $\times 10^{-5}$ $M_\odot\,{\rm yr}^{-1}$ in itself cannot explain the massive shell SN 2014C interacted with. Though a short W-R phase will sweep up a dense shell close to the star, the shell will not have much mass because the RSG wind was expanding freely at this small radius. A possible solution is if the short W-R phase was accompanied with an enhanced mass loss rate (e.g., $\sim 10^{-3}$ $M_\odot$ yr^{-1}), which is a scenario proposed by Chugai & Chevalier (2006) for SN 2001em.

3.4.2. *Shell ejection in a single eruption*

Alternatively, in light of the established connection between type IIn supernovae and LBV stars, it is plausible that the shell surrounding the SN 2014C progenitor system was ejected in a single eruptive event rather than a brief period of enhanced W-R stellar wind. Shell ejections have typical velocities of $\gtrsim 100$ km s^{-1}, which would mean that the major mass loss event would have taken place in the last $\lesssim 100$ years prior to core collapse.

Providing the pre-explosion source was a massive star cluster, the most probable turn-off mass range estimated from the BPASS models ($3.5 - 9.5$ $M_\odot$) is too low to be compatible with typical LBV progenitors ($M_{ZAMS} \gtrsim 20 M_\odot$). However, because uncertainties in our fitting allow room for ages as low as 10 Myr, an LBV-like progenitor is not ruled out completely. It is worth noting that the type IIn-LBV connection is thus far only robust for stars with H-rich envelopes and to date there is no direct detection of the progenitor star of an interacting H-poor supernova. Indirect arguments that the progenitors of type Ibn supernovae exploded in the transition from LBV to W-R phases (Foley et al. 2007; Pastorello et al. 2007; Smith et al. 2012), potentially due to instabilities initiated in the final stages of He core

burning (Pastorello et al. 2015), have been advanced.

Ejection of an H-rich common envelope in a binary system is also a plausible scenario. Stellar evolution calculations and population models that incorporate stellar duplicity show that stars less than 20 $M_\odot$ in interacting binaries can be stripped of their hydrogen envelopes via mass transfer to a companion and/or the loss of the common envelope, and end their lives as low mass helium stars that explode as SN Ibc (Yoon et al. 2010; Eldridge et al. 2013). This type of progenitor system was proposed for the type Ib iPTF13bvn (Eldridge et al. 2015), which has an optical spectrum at maximum light very similar to that of SN 2014C (see Figure 4).

3.4.3. *CSM confinement*

The location of SN 2014C's progenitor star within a compact massive star cluster makes it plausible that hot gas from stellar winds and prior supernovae could have provided a large external pressure by which to confine the RSG wind into a shell near the star. Simulations have shown that it is difficult to confine RSG wind to < 0.3 pc with external thermal or ram pressure (van Marle et al. 2006; Eldridge et al. 2006), thus this scenario is not plausible unless the wind had considerable asymmetry originating from stellar rotation and/or duplicity (Eldridge 2007).

A viable alternative scenario is through the process of photoionization-confinement. Mackey et al. (2014) demonstrate how an external radiation field generated by neighboring stars can form a standing shock in the neutral part of an outflowing wind and create an almost static, photoionization-confined shell that traps up to 35 per cent of all mass lost during the RSG phase close to the star until it explodes. Their model was specific to Betelgeuse and its $\sim 0.1\ M_\odot$ circumstellar shell, but the model is applicable to other stars that might have much more massive shells.

Complicating this interpretation is the fact that the progenitor star of SN 2014C was H-stripped at the time of explosion and thus no longer in the RSG phase. If the star evolved through a W-R phase with a typical timescale of $\sim 10^5$ yr, the momentum of the winds traveling $\gtrsim 1000$ km s^{-1} make it unlikely that a shell $\lesssim 1\ M_\odot$ in mass with radius $\sim 3 \times 10^{16}$ cm would have survived. The photoionization-confined shell scenario remains plausible if the shell was initially much more massive at the end of the RSG phase (a few $\times 1\ M_\odot$) and/or if the W-R phase was short.

4. CONCLUSION

We have presented spectroscopic observations of SN 2014C that follow its evolution from an ordinary type Ib supernova to an interacting type IIn. Our observations are consistent with the supernova having exploded in a cavity before encountering a dense, nearby ($\gtrsim 3 \times 10^{16}$ cm) H-rich shell formed from mass lost from the progenitor star. We considered three possible origins to the shell: 1) a W-R fast wind phase that overtook a slower RSG wind, 2) an eruptive ejection, or 3) various forms of CSM confinement. We find that all explanations require that the progenitor star experienced a brief $\lesssim 1000$ yr W-R phase. The brief W-R phase may have been associated with larger-than-normal mass loss rates ($> 10^{-4}\ M_\odot$ yr^{-1}). Alternatively, the prior RSG wind may have been distributed asymmetrically and/or confined via a photoionization layer. Our observations disfavor a sudden eruption in an LBV-like event, but do not rule out such a scenario. Ejection of an H-rich common envelope in a binary system is also possible.

We also presented archival Subaru and HST pre-explosion images covering the field of SN 2014C that show a luminous coincident source. The SED and source size as measured by HST are both consistent with a compact massive star cluster. We estimated the age of the cluster to be $30 - 300$ Myr, and favor models incorporating interacting binary systems with ages closer to 30 Myr in light of relatively strong Hα emission.

Because extensive archival data of the host galaxy exist, it is possible that a historical light curve could be constructed. Such a light curve could be used to look for changes in apparent brightness in the system that may be associated with precursor activity from an unstable massive star (see, e.g., Pastorello et al. 2013 and Ofek et al. 2014). Notably, SN 2013bu was discovered in NGC 7331 on 2013 April 21 (Itagaki et al. 2013), which was only eight months before the discovery of SN 2014C. Thus, multi-epoch observations of SN 2013bu that cover the region of SN 2014C would be appropriate for this type of archival analysis.

We searched for previous HST observations, but unfortunately SN 2014C fell slightly outside the footprint except for the F658N images presented here. Future observations can pinpoint the location within the host cluster and investigate the immediate stellar environment when the supernova has faded. Our results strongly motivate observations at ultraviolet wavelengths from which line diagnostics can be performed to investigate potentially enhanced abundances consistent with CNO processed material (e.g., Fransson et al. 2002, 2014). It is anticipated that additional emission lines will develop as the CSM cools over time (see, e.g., SN 2005ip; Smith et al. 2009). Line diagnostics at these wavelengths would reveal important information about the evolutionary transitions a massive star may undergo in its final stages approaching core collapse.

SN 2014C is a well-observed example of a class of core-collapse supernovae that fill a gap between events that interact strongly with nearby environments immediately after explosion (type IIn and Ibn) and events that are never observed to interact at all (the majority of SN Ibc). Previous surveys of late-time radio emission from SN Ibc suggest that events like SN 2014C are infrequent (Bietenholz et al. 2014). However, considering that these follow-up observations are not densely sampled and cover many SN Ibc that are > 50 Mpc, the frequency of other late interaction events where the mass lost is less extreme and/or concentrated at greater distances is unknown.

The shell of mass loss material surrounding the progenitor star of SN 2014C was close enough to be detected via subsequent interaction with the blast wave, and yet fortuitously distant enough to permit a clear view of the underlying supernova. Improved constraints on the frequency with which SN Ibc interact with their stripped shells can contribute important information about the final stages of mass loss and stellar evolution. Given that the hydrodynamic instabilities that lead to enhanced pre-supernova mass loss may be related to deviations

from spherical symmetry in the progenitor star structure (Smith & Arnett 2014), understanding how the underlying physical mechanisms may permit a range of pre-supernova mass loss rates and time lags may also help with our understanding of the core collapse process itself.

We thank an anonymous referee who provided many helpful comments and suggestions that improved the quality and presentation of this paper. Observations reported here were obtained at the MMT Observatory, a joint facility of the Smithsonian Institution and the University of Arizona, as well as the 6.5 m Magellan Telescopes located at Las Campanas Observatory, Chile. This paper uses data taken with the MODS spectrographs built with funding from NSF grant AST-9987045 and the NSF Telescope System Instrumentation Program (TSIP), with additional funds from the Ohio Board of Regents and the Ohio State University Office of Research. Based in part on data collected at Subaru Telescope and obtained from the SMOKA, which is operated by the Astronomy Data Center, National Astronomical Observatory of Japan. Some of the data presented in this paper were obtained from the Mikulski Archive for Space Telescopes (MAST). STScI is operated by the Association of Universities for Research in Astronomy, Inc., under NASA contract NAS5-26555. Support for MAST for non-HST data is provided by the NASA Office of Space Science via grant NNX09AF08G and by other grants and contracts. This paper made use of the Weizmann interactive supernova data repository (WISEREP) - http://wiserep.weizmann.ac.il. J. M. acknowledges support from the Deutsche Forschungsgemeinschaft priority program 1573, Physics of the Interstellar Medium. D. M. thanks M. Shara and A. Pagnotta for helpful discussions.

REFERENCES

Aldering, G., Humphreys, R. M., & Richmond, M. 1994, AJ, 107, 662
Asplund, M., Grevesse, N., & Sauval, A. J. 2005, in Astronomical Society of the Pacific Conference Series, Vol. 336, Cosmic Abundances as Records of Stellar Evolution and Nucleosynthesis, ed. T. G. Barnes III & F. N. Bash, 25–+
Bastian, N., Schweizer, F., Goudfrooij, P., Larsen, S. S., & Kissler-Patig, M. 2013, MNRAS, 431, 1252
Bauer, F. E., Dwarkadas, V. V., Brandt, W. N., et al. 2008, ApJ, 688, 1210
Bersten, M. C., Benvenuto, O. G., Folatelli, G., et al. 2014, AJ, 148, 68
Bianco, F. B., Modjaz, M., Hicken, M., et al. 2014, ApJS, 213, 19
Bietenholz, M. F., & Bartel, N. 2005, ApJ, 625, L99
—. 2007, ApJ, 665, L47
Bietenholz, M. F., De Colle, F., Granot, J., Bartel, N., & Soderberg, A. M. 2014, MNRAS, 440, 821
Branch, D., Jeffery, D. J., Young, T. R., & Baron, E. 2006, PASP, 118, 791
Branch, D., Benetti, S., Kasen, D., et al. 2002, ApJ, 566, 1005
Cao, Y., Kasliwal, M. M., Arcavi, I., et al. 2013, ApJ, 775, L7
Cardelli, J. A., Clayton, G. C., & Mathis, J. S. 1989, ApJ, 345, 245
Chevalier, R. A., & Fransson, C. 2006, ApJ, 651, 381
Chugai, N. N., & Chevalier, R. A. 2006, ApJ, 641, 1051
Chugai, N. N., & Danziger, I. J. 1994, MNRAS, 268, 173
Claeys, J. S. W., de Mink, S. E., Pols, O. R., Eldridge, J. J., & Baes, M. 2011, A&A, 528, A131
Crowther, P. A. 2007, ARA&A, 45, 177
de Witt, A., Bietenholz, M. F., Kamble, A., et al. 2015, ArXiv e-prints, arXiv:1503.00837
Deng, J. S., Qiu, Y. L., Hu, J. Y., Hatano, K., & Branch, D. 2000, ApJ, 540, 452
Dessart, L., Hillier, D. J., Woosley, S., et al. 2015, MNRAS, 453, 2189
Drout, M. R., Soderberg, A. M., Gal-Yam, A., et al. 2011, ApJ, 741, 97
Dwarkadas, V. V. 2011, MNRAS, 412, 1639
Eldridge, J. J. 2007, MNRAS, 377, L29
Eldridge, J. J., Fraser, M., Maund, J. R., & Smartt, S. J. 2015, MNRAS, 446, 2689
Eldridge, J. J., Fraser, M., Smartt, S. J., Maund, J. R., & Crockett, R. M. 2013, MNRAS, 436, 774
Eldridge, J. J., Genet, F., Daigne, F., & Mochkovitch, R. 2006, MNRAS, 367, 186
Eldridge, J. J., Izzard, R. G., & Tout, C. A. 2008, MNRAS, 384, 1109
Eldridge, J. J., & Stanway, E. R. 2009, MNRAS, 400, 1019
Fabricant, D., Cheimets, P., Caldwell, N., & Geary, J. 1998, PASP, 110, 79
Fesen, R. A., & Hurford, A. P. 1996, ApJS, 106, 563
Fesen, R. A., Gerardy, C. L., Filippenko, A. V., et al. 1999, AJ, 117, 725
Filippenko, A. V. 1997, ARA&A, 35, 309
Filippenko, A. V., & Chornock, R. 2001, IAU Circ., 7737, 3
Foley, R. J., Smith, N., Ganeshalingam, M., et al. 2007, ApJ, 657, L105
Fransson, C., Chevalier, R. A., Filippenko, A. V., et al. 2002, ApJ, 572, 350
Fransson, C., Ergon, M., Challis, P. J., et al. 2014, ApJ, 797, 118
Freedman, W. L., Madore, B. F., Gibson, B. K., et al. 2001, ApJ, 553, 47
Fremling, C., Sollerman, J., Taddia, F., et al. 2014, A&A, 565, A114
Gal-Yam, A., & Leonard, D. C. 2009, Nature, 458, 865
Garcia-Segura, G., Langer, N., & Mac Low, M.-M. 1996, A&A, 316, 133
Gaskell, C. M., Cappellaro, E., Dinerstein, H. L., et al. 1986, ApJ, 306, L77
Granot, J., & Ramirez-Ruiz, E. 2004, ApJ, 609, L9
Groh, J. H., Georgy, C., & Ekström, S. 2013, A&A, 558, L1
Gusev, A. S., Pilyugin, L. S., Sakhibov, F., et al. 2012, MNRAS, 424, 1930
Hachinger, S., Mazzali, P. A., Taubenberger, S., et al. 2012, MNRAS, 422, 70
Harkness, R. P., Wheeler, J. C., Margon, B., et al. 1987, ApJ, 317, 355
Heger, A., Fryer, C. L., Woosley, S. E., Langer, N., & Hartmann, D. H. 2003, ApJ, 591, 288
Humason, M. L. 1959, IAUC, 1682, 1
Hwang, U., & Laming, J. M. 2009, ApJ, 703, 883
Itagaki, K., Noguchi, T., Nakano, S., et al. 2013, Central Bureau Electronic Telegrams, 3498, 1
Jordi, K., Grebel, E. K., & Ammon, K. 2006, A&A, 460, 339
Kallman, T. R., & McCray, R. 1982, ApJS, 50, 263
Kamble, A., Margutti, R., Soderberg, A. M., et al. 2015, ArXiv e-prints, arXiv:1504.07988
Kim, M., Zheng, W., Li, W., et al. 2014, Central Bureau Electronic Telegrams, 3777, 1
Kotak, R., & Vink, J. S. 2006, A&A, 460, L5
Krauss, M. I., Soderberg, A. M., Chomiuk, L., et al. 2012, ArXiv e-prints, arXiv:1201.0770
Landi, E., Young, P. R., Dere, K. P., Del Zanna, G., & Mason, H. E. 2013, ApJ, 763, 86
Langer, N. 2012, ARA&A, 50, 107
Langer, N., Hamann, W.-R., Lennon, M., et al. 1994, A&A, 290, 819
Lawrence, S. S., Sugerman, B. E., Bouchet, P., et al. 2000, ApJ, 537, L123
Mackey, J., Mohamed, S., Gvaramadze, V. V., et al. 2014, Nature, 512, 282
Maeda, K., Katsuda, S., Bamba, A., Terada, Y., & Fukazawa, Y. 2014, ApJ, 785, 95
Maeda, K., Hattori, T., Milisavljevic, D., et al. 2015, ApJ, 807, 35
Maeder, A., & Meynet, G. 2000, ARA&A, 38, 143

Margutti, R., Milisavljevic, D., Soderberg, A. M., et al. 2014, ApJ, 780, 21
Massey, P., Neugent, K. F., & Morrell, N. 2015, ApJ, 807, 81
Massey, P., Neugent, K. F., Morrell, N., & Hillier, D. J. 2014, ApJ, 788, 83
Matheson, T., Filippenko, A. V., Li, W., Leonard, D. C., & Shields, J. C. 2001, AJ, 121, 1648
Mauerhan, J. C., Smith, N., Filippenko, A. V., et al. 2013, MNRAS, 430, 1801
Maund, J. R., Fraser, M., Ergon, M., et al. 2011, ApJ, 739, L37
Meynet, G., Maeder, A., Schaller, G., Schaerer, D., & Charbonnel, C. 1994, A&AS, 103, 97
Milisavljevic, D., Fesen, R. A., Chevalier, R. A., et al. 2012, ApJ, 751, 25
Milisavljevic, D., Margutti, R., Soderberg, A. M., et al. 2013, ApJ, 767, 71
Milisavljevic, D., Margutti, R., Parrent, J. T., et al. 2015, ApJ, 799, 51
Miller, G. J., & Chu, Y.-H. 1993, ApJS, 85, 137
Miyazaki, S., Komiyama, Y., Sekiguchi, M., et al. 2002, PASJ, 54, 833
Modjaz, M., Li, W., Butler, N., et al. 2009, ApJ, 702, 226
Modjaz, M., Blondin, S., Kirshner, R. P., et al. 2014, AJ, 147, 99
Monet, D. G., Levine, S. E., Canzian, B., et al. 2003, AJ, 125, 984
Moriya, T. J. 2015, ApJ, 803, L26
Ofek, E. O., Sullivan, M., Cenko, S. B., et al. 2013, Nature, 494, 65
Ofek, E. O., Sullivan, M., Shaviv, N. J., et al. 2014, ApJ, 789, 104
Osterbrock, D. E., & Ferland, G. J. 2006, Astrophysics of gaseous nebulae and active galactic nuclei, 2nd edn. (Sausalito, CA: University Science Books)
Parrent, J. T., Milisavljevic, D., Soderberg, A. M., & Parthasarathy, M. 2015, ArXiv e-prints, arXiv:1505.06645
Pastorello, A., Smartt, S. J., Mattila, S., et al. 2007, Nature, 447, 829
Pastorello, A., Cappellaro, E., Inserra, C., et al. 2013, ApJ, 767, 1
Pastorello, A., Benetti, S., Brown, P. J., et al. 2015, MNRAS, 449, 1921
Pettini, M., & Pagel, B. E. J. 2004, MNRAS, 348, L59
Podsiadlowski, P., Joss, P. C., & Hsu, J. J. L. 1992, ApJ, 391, 246
Pogge, R. W., Atwood, B., Brewer, D. F., et al. 2010, in Society of Photo-Optical Instrumentation Engineers (SPIE) Conference Series, Vol. 7735, Society of Photo-Optical Instrumentation Engineers (SPIE) Conference Series, 0
Puls, J., Vink, J. S., & Najarro, F. 2008, A&A Rev., 16, 209
Quataert, E., & Shiode, J. 2012, MNRAS, 423, L92
Sanders, N. E., Soderberg, A. M., Levesque, E. M., et al. 2012, ApJ, 758, 132
Schinzel, F. K., Taylor, G. B., Stockdale, C. J., Granot, J., & Ramirez-Ruiz, E. 2009, ApJ, 691, 1380
Schlafly, E. F., & Finkbeiner, D. P. 2011, ApJ, 737, 103
Schmidt, G. D., Weymann, R. J., & Foltz, C. B. 1989, PASP, 101, 713
Schure, K. M., Vink, J., García-Segura, G., & Achterberg, A. 2008, ApJ, 686, 399
Shara, M. M., Bibby, J. L., Zurek, D., et al. 2013, AJ, 146, 162
Shaw, R. A., & Dufour, R. J. 1994, in Astronomical Society of the Pacific Conference Series, Vol. 61, Astronomical Data Analysis Software and Systems III, ed. D. R. Crabtree, R. J. Hanisch, & J. Barnes, 327
Smartt, S. J. 2009, ARA&A, 47, 63
Smith, N. 2014, ARA&A, 52, 487
Smith, N., & Arnett, W. D. 2014, ApJ, 785, 82
Smith, N., Li, W., Filippenko, A. V., & Chornock, R. 2011, MNRAS, 412, 1522
Smith, N., Mauerhan, J. C., & Prieto, J. L. 2014, MNRAS, 438, 1191
Smith, N., Mauerhan, J. C., Silverman, J. M., et al. 2012, MNRAS, 426, 1905
Smith, N., & Owocki, S. P. 2006, ApJ, 645, L45
Smith, N., Silverman, J. M., Chornock, R., et al. 2009, ApJ, 695, 1334
Soderberg, A. M., Gal-Yam, A., & Kulkarni, S. R. 2004, GRB Coordinates Network, 2586, 1
Soderberg, A. M., Berger, E., Page, K. L., et al. 2008, Nature, 453, 469
Sonneborn, G., Pun, C. S. J., Kimble, R. A., et al. 1998, ApJ, 492, L139
Srivastav, S., Anupama, G. C., & Sahu, D. K. 2014, MNRAS, 445, 1932
Stockdale, C. J., Van Dyk, S. D., Sramek, R. A., et al. 2004, IAU Circ., 8282, 2
Stritzinger, M., Taddia, F., Fransson, C., et al. 2012, ApJ, 756, 173
Taddia, F., Sollerman, J., Fremling, C., et al. 2015, ArXiv e-prints, arXiv:1505.04719
Tanaka, M., Yamanaka, M., Maeda, K., et al. 2009, ApJ, 700, 1680
Thilker, D. A., Boissier, S., Bianchi, L., et al. 2007, ApJS, 173, 572
Thomas, R. C., Nugent, P. E., & Meza, J. C. 2011, PASP, 123, 237
Turatto, M., Benetti, S., & Cappellaro, E. 2003, in From Twilight to Highlight: The Physics of Supernovae, ed. W. Hillebrandt & B. Leibundgut, 200
van Dyk, S. D. 2010, in Astronomical Society of the Pacific Conference Series, Vol. 425, Hot and Cool: Bridging Gaps in Massive Star Evolution, ed. C. Leitherer, P. D. Bennett, P. W. Morris, & J. T. Van Loon, 73
Van Dyk, S. D., Li, W., & Filippenko, A. V. 2003, PASP, 115, 1
Van Dyk, S. D., Zheng, W., Fox, O. D., et al. 2014, AJ, 147, 37
van Marle, A. J., Langer, N., Achterberg, A., & García-Segura, G. 2006, A&A, 460, 105
Vink, J. S., & de Koter, A. 2005, A&A, 442, 587
Vink, J. S., de Koter, A., & Lamers, H. J. G. L. M. 2001, A&A, 369, 574
Wellstein, S., & Langer, N. 1999, A&A, 350, 148
Wellstein, S., Langer, N., & Braun, H. 2001, A&A, 369, 939
Woosley, S. E., Blinnikov, S., & Heger, A. 2007, Nature, 450, 390
Woosley, S. E., Langer, N., & Weaver, T. A. 1995, ApJ, 448, 315
Yaron, O., & Gal-Yam, A. 2012, PASP, 124, 668
Yoon, S.-C., & Cantiello, M. 2010, ApJ, 717, L62
Yoon, S.-C., Woosley, S. E., & Langer, N. 2010, ApJ, 725, 940